Chalcogenide Letters Vol. 12, No. 5, May 2015, p. 263 - 275

INFLUENCE OF THERMAL ANNEALING ON STRUCTURAL AND OPTICAL PROPERTIES OF $Se_{70}Te_{15}Sb_{15}$ THIN FILMS

M. A. ABDEL-RAHIM, M. M. HAFIZ, A. Z. MAHMOUD*
Physics Department, Faculty of Science, Assiut University, Assiut 71516, Egypt.

The effect of thermal annealing on the structural and optical properties of $Se_{70}Te_{15}$ Sb_{15} thin films was investigated. X-ray diffraction (XRD) patterns revealed that the as-deposited films were amorphous in nature. Analyzing the XRD patterns and the morphology of the scanning electron microscopy (SEM) of the annealed films show improved crystallinity with increasing annealing temperature. Particle size and crystallinity increased but the dislocation density and strain decreased with increasing annealing temperature. The indirect optical energy gap decreased with increasing the annealing temperature. The refractive index, n, and the extinction coefficient, k_{ex}, increased with increasing the annealing temperature. Dispersion of refractive index was described using Wemple-Didomenico (WDD) single oscillator model. The dispersion parameters, the high frequency dielectric constant and the ratio of the free carrier concentration to its effective mass N/m^* are sensitive to the annealing temperature. These results are discussed and correlated in terms of amorphous-crystalline transformation.

(Received April 2, 2015; Accepted May 14, 2015)

Keywords: Optical constants; Thin Films; X-Ray Diffraction (XRD); Scanning Electron Microscopy (SEM)

1. Introduction

During the last three decades, Chalcogenide glasses have attracted much attention because of their potential application in solid-state devices. Impurity effects in chalcogenide glasses its important in fabricating glassy semiconductors. Moreover, they represents good core materials of optical fibers for transmission especially when short length and flexibility are required [1- 4]. The current interest in chalcogenide materials centers on x-ray imaging and photonics [5].

Selenium –based Chalcogenide glasses have high transparency in the broad middle and far IR regions as well as strong non-linear properties [6]. Apart from these applications, amorphous Se has been found to have tremendous potential in Xeroxing applications and therefore several attempts have been made to improve its properties by alloying it with other elements. Alloying elements produce characteristic effects depending on the electronic structure of these elements [7].

The Se-Te glassy alloy system based on Se is considered as commercial product. Also, it has a scientific and technological importance. They are widely used for various applications as optical recording media, because of their excellent laser writing, sensitivity, xerography and electrographic applications. However, thermal instability leading to crystallization is found to be one of the drawbacks of these alloys. Hence, an attempts has been made to improve the stability of Se-Te by addition of a third element [8- 10].

The addition of a third element such as Sb to the binary Chalcogenide Se-Te system produces stable glassy alloys [9- 11]. However, the addition of the third element expands the glass forming area and also creates compositional and configurationally disorder in the system. Moreover, it is observed that the addition of the third element helps in getting cross-linked

*Corresponding author: amerazain@yahoo.com.

structure and consequently increasing the glass transition and crystallization temperature of the binary alloy [9, 12, 13].

Thermal processes are important in inducing crystallization in chalcogenide glasses. The optical storage based on the amorphous-crystalline phase transition utilizes large optical reflectivity and optical absorption changes obtained in some semiconductors-semimetals thin films by heat treatment. Several researchers [11, 14- 16] have studied the effect of thermal annealing on structural, electrical and optical properties of Chalcogenide glasses.

The present work reports the effect of heat treatment on the structural and optical properties of $Se_{70}Te_{15}Sb_{15}$. X-ray diffraction (XRD) and scanning electron microscopy (SEM) were used to study the structural changes for the studied composition annealed at different temperatures for one hour. The effect of the thermal annealing on the optical properties was interpreted based on the density of states model in amorphous materials proposed by Mott and Davis [17].

2. Experimental

Bulk $Se_{70}Te_{15}Sb_{15}$ glass was prepared by the well known melting quench technique. Appropriate amounts of high purity (99.999 %) Se, Te and Sb (from Aldrich UK) were weighed (10 g total weight) according to their atomic percentage. The weighed elements were placed into a quartz glass ampoule and sealed under vacuum of 10^{-4} Torr. The sealed ampoule was heated in Heraus programmable tube furnace (type RO7115). The heating rate was approximately 3-5 K/min. The temperature was kept at 950 K for 24 h. The long periods of synthesis and frequently rocking of the melt were necessary for homogeneity of the material composition. The molten materials were then rapidly quenched in ice water mixture to obtain a sample in a glassy state. Thin films were prepared by thermal evaporation under vacuum of 10^{-5} Torr using Edwards E306 coating unit. A constant evaporation rate (3 nm/s) was used to deposit the films. The evaporation rates as well as the films thickness were controlled using quartz crystal monitor (FTMS). The films were checked using the energy dispersive spectroscopy (EDAX) technique. The atomic percentage ratios of the films are very close to their bulk sample.

The glassy natures of as-deposited as well as the crystalline phase structures for annealed samples were identified using a Philips diffractometer type 1710. The surface morphology of the films was investigated by using scanning electron microscopy (SEM) technique, Jeol (JSM)-T200 type. The transmittance, T, and reflectance, R, of the thin films were measured using the double beam spectrophotometer type (Shimadzu 2101, Japan) in the wavelength range 200–2500 nm.

3. Results and discussion:

3.1 Structural analysis

A typical DSC trace of $Se_{70}Te_{15}Sb_{15}$ glass powder recorded at heating rate 15 K/min is shown in Fig. 1. The glass transition temperature, T_g, and the crystallization temperature, T_p, were determined using the microprocessor of the thermal analyzer. The DSC curves show a first exothermic effect followed by strong exothermic peak which are partially overlapped. On the other hand, the appearance of an endothermic hum in DSC trace is corresponding to the glass transition which resulted from large viscosity changes. These large viscosity changes occur during the material transformation from amorphous phase to supper-cooled liquid state. The appearance of a double glass transition at T_{g1} and T_{g2} indicates unusual phase separation occurring in this glassy alloy. The glass transition temperatures (T_{g1} and T_{g2}) and the crystallization temperatures (T_{p1} and T_{p2}) are found 351, 368, 401 and 413 K respectively. The annealing temperatures were selected to range between the glass transition and crystallization temperatures for the studied composition.

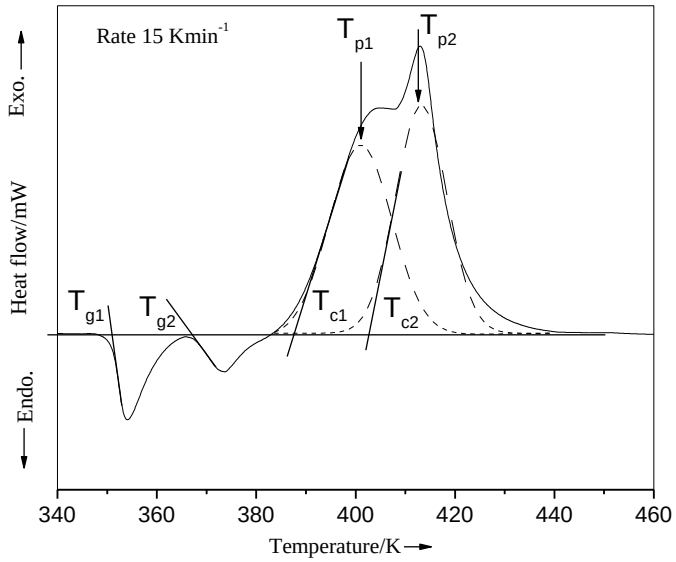

Fig. 1 DSC curves of $Se_{70}Te_{15}Sb_{15}$ glass measured at heating rates 15K/min.

The morphology of the annealed $Se_{70}Te_{15}Sb_{15}$ thin films at different temperatures for one hour are shown in Fig. 2(a, b). The samples were coated with gold before SEM examination to study the surface morphology. Gold coating was used to prevent electrical charging of the specimens. The microstructure of the annealed sample at 383 K is shown in Fig. 2(a). A polycrystalline structure consists of different phases of spherically shaped with different sizes are embedded in the glassy matrix. Further increase of the annealing temperature (423 K) reveals that the amount of the transformed crystalline phase increased and the crystallized particles increase in size as shown in Fig. 2(b).

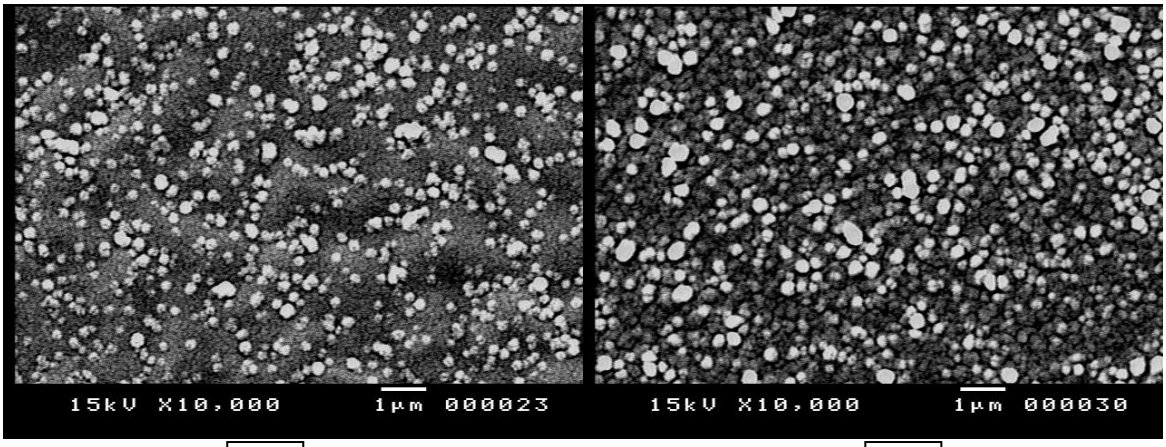

Fig. 2. SEM micrograph of $Se_{70}Te_{15}Sb_{1.5}$ thin films annealed at (a) 383 K (b) 423 K for 1 hour.

In order to determine the crystalline phases that appeared in DSC and SEM for the annealed $Se_{70}Te_{15}Sb_{15}$ thin films, the x-ray diffraction pattern of the films were analyzed. Fig 3 shows XRD pattern of the as-deposited and annealed $Se_{70}Te_{15}Sb_{15}$ thin films. As shown in this figure, the absence of sharp structural peaks in these patterns confirmed the amorphous glassy nature of the as-deposited film. However, the films annealed in N_2 atmosphere at 363, 383, 403

and 423 K for one hour showed a polycrystalline structure indicating an amorphous to crystalline phase transition. The analysis of the XRD patterns for all annealed films as shown in Fig. 3 show that the dominant crystalline phases are $SeTe_2Sb_2$ and $Se_{0.96}Te_{0.04}$ according to ASTM files. As shown in Fig. 3, the major phase formation is very sensitive to the annealing process and the diffraction peak intensities increase with increasing annealing temperature, which indirectly indicate the improvement of the crystallization with increasing the annealing temperature.

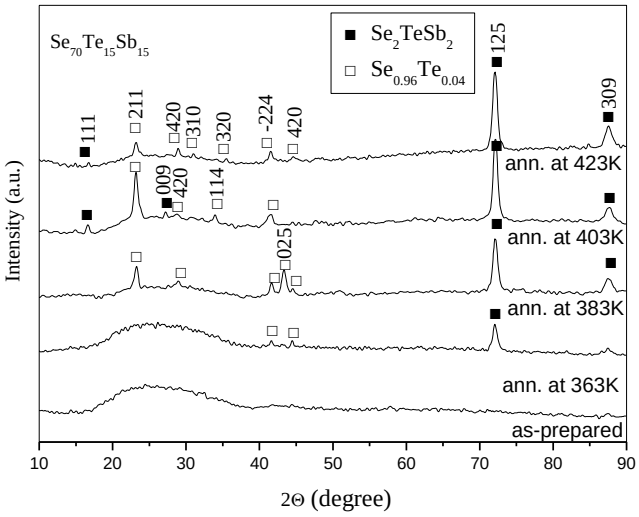

Fig. 3. X-ray diffraction patterns of $Se_{70}Te_{15}Sb_{15}$ for as-prepared and annealed films.

The average crystallite size (D) of the annealed films was calculated using Scherrer's equation [18]:

$$D = \frac{0.94\lambda}{\beta \cos\theta}, \tag{1}$$

where λ is the wavelength used, β is the angular line width at half maximum intensity (FWHM) in radiant and θ is the Bragg's angle. The average sizes of crystallites, D, values for $SeTe_2Sb_2$ phase are in nanometer scale and found to change from 13.58 to 16.35 nm for $SeTe_2Sb_2$ phase when the annealing temperature increased from 363 to 423 K as shown in Table 1. On the other hand, the dislocation density, δ, is defined as the length of the dislocation lines per unit volume of the crystal and is given by $\delta = 1/D^2$, while, the strain value (ε) is calculated from the following relation [19, 20]

$$\varepsilon = \left[\frac{\lambda}{D\cos\theta} - \beta\right]\frac{1}{\tan\theta} \tag{2}$$

Table 1. The crystallite size, D, srain, ε, and dislocation density, δ, for annealed $Se_{70}Te_{15}Sb_{15}$ films for one hour at different temperature

phase	**Annealing Temp. (K)**	**Crystallite size(D) (nm)**	**Strain(ε)**	**dislocation density(δ) $\times 10^{15}$ (m^{-2})**
$SeTe_2Sb_2$	363	13.58	0.00117	5.42
	383	14.51	0.0011	4.75
	403	15.75	0.00101	4.03
	423	16.37	9.73E-4	3.73

The deduced δ and ε are listed in Table 1. It is observed that the strain and dislocation density decreases with increasing the annealing temperature. These results are in agreement with the previous work [8, 21-23].

3.2 Optical properties

3.2.1 Absorption coefficient

The optical constants were deduced from the transmittance, $T(\lambda)$, and reflectance, $R(\lambda)$, spectral. Fig. 4(a, b) shows the spectra distribution of the transmittance and reflectance for as-deposited and annealed $Se_{70}Te_{15}Sb_{15}$ thin films in the range 200-2500 nm. It could be noted from Fig. 4 that the fundamental absorption edge was shifted to higher wavelength with increasing the annealing temperature. Furthermore, the transmittance decreases with increasing the annealing temperature. The reflectance showed opposite behavior to this in the transmittance spectrum. The observed decrease in the transmittance which is accompanied by the structural transformation of the film with annealing [24, 25].

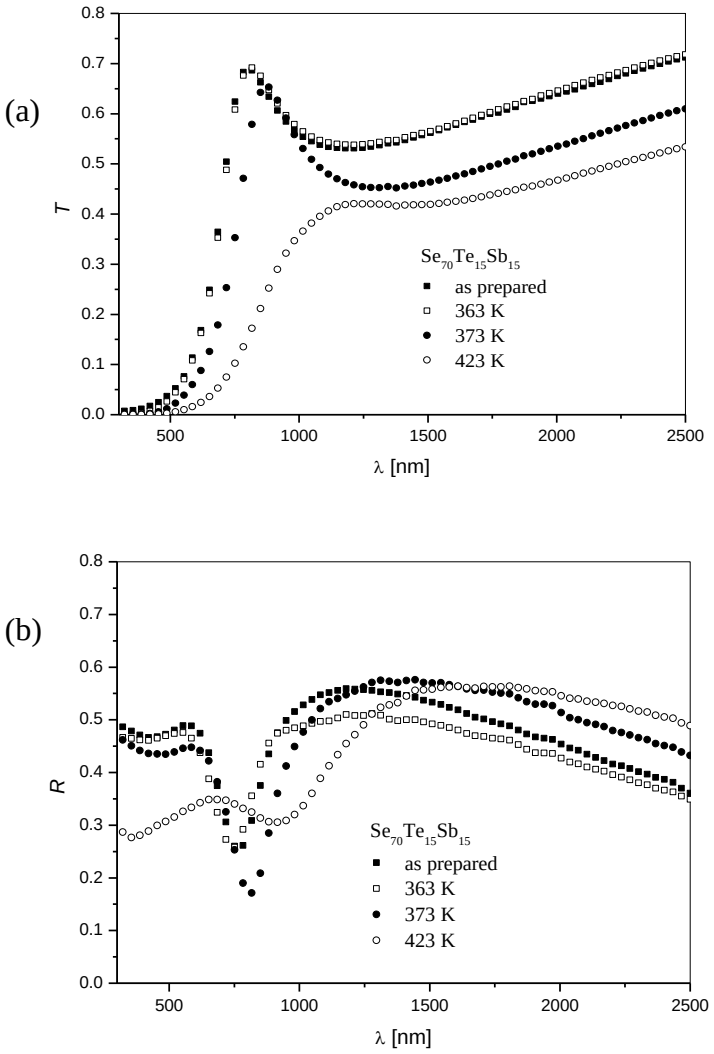

Fig. 4. a) Transmission, T, spectra. b) Reflection, R, spectra for as-deposited and annealed $Se_{70}Te_{15}Sb_{15}$ thin films at different annealing temperature for 1 h.

The absorption coefficient, α, is one of the most significant parameters in semiconducting thin films. This parameter can be deduced from the experimentally measured values of the transmittance, *T*, and reflectance, *R*, by using the relation [26]

$$\alpha = \frac{1}{d} ln \left[\frac{(1-R)^2}{T}\right], \tag{3}$$

where d is the film thickness.

Fig. 5 shows the dependence of the absorption coefficient, α, on the incident photon energy ($h\nu$) for as-deposited and annealed $Se_{70}Te_{15}Sb_{15}$ thin films. It is observed that the values of the absorption coefficient increases with increasing both the photon energy and annealing temperature. The increase in the absorption coefficient is due to the size effect [25].

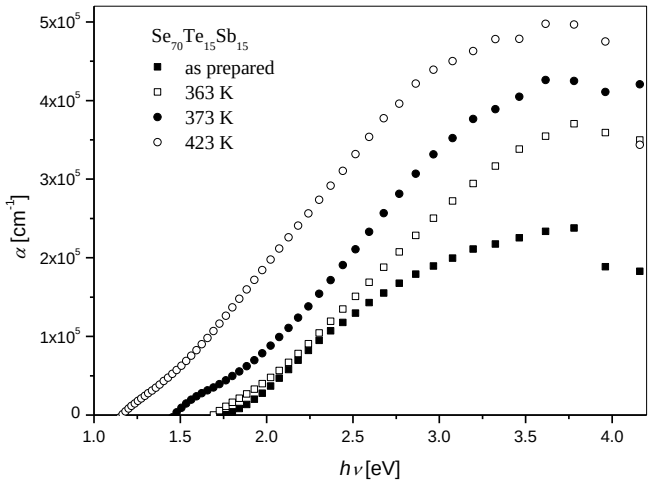

Fig. 5. The variation of the absorption coefficient, α, with the photon energy, hν, for as-deposited and annealed $Se_{70}Te_{15}Sb_{15}$ thin films at different annealing temperature for 1 h.

In the high absorption region (α >10^4 cm^{-1}) the absorption is characterized by the following equation [27, 28]

$$(\alpha h\nu) = B\left(h\nu - E_g\right)^r, \tag{4}$$

where ν is the frequency of the incident beam, B is a constant that depends on the transition probability, E_g is the optical band gap and r is a parameter that depends on the transition process for a material having one kind of transition, the value of r is ½ for the direct allowed transition and the value of 2 for indirect allowed transition. The dependency of $(\alpha h\nu)^{1/r}$ on photon energy was plotted for different values of r and showed that the transition has indirect allowed transition for the studied composition.

Fig. 6 shows the plots of $(\alpha h\nu)^{1/2}$ versus $(h\nu)$ for the studied composition. The optical energy gap, E_g, are obtained by extrapolating the linear portions of the plots to intersect the energy axis.

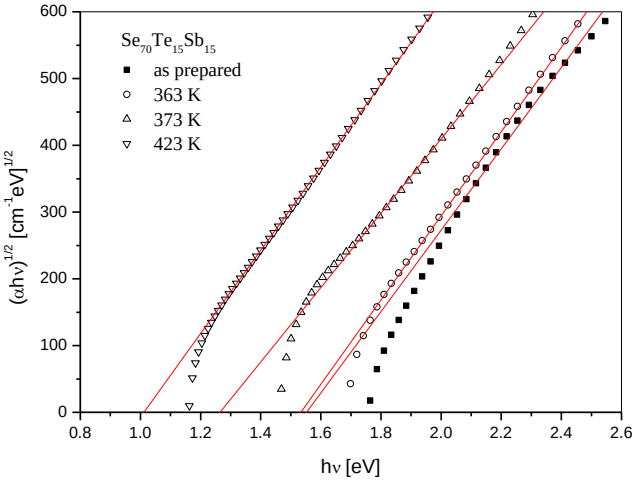

Fig. 6. Plot of $(\alpha h\nu)^{1/2}$ versus $h\nu$ for $Se_{70}Te_{15}Sb_{15}$ thin film at different annealing temperature for 1h.

It is noticed that the optical energy gap, E_g, decreases slightly with increasing the annealing temperature up to 360 K and sharply decreased with further increasing the annealing temperature as shown in Fig. 7. The crystallite size increased and the strain values decreased with increasing the annealing temperature. This leads to decreasing the optical energy gap [29, 30].

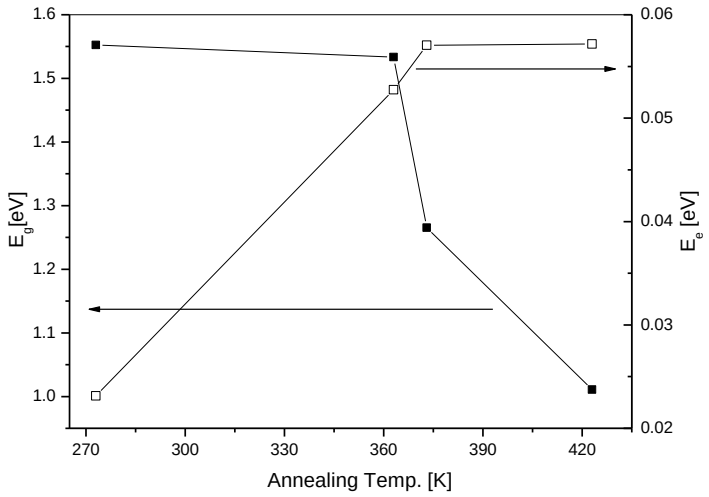

Fig. 7. The values of E_g and E_e as a function of annealing temperature for $Se_{70}Te_{15}Sb_{15}$ thin films.

In the low absorption region ($\alpha < 10^4$ cm^{-1}), there is usually an Urbach tail [31] where $\alpha(\nu)$ depends exponentially on the photon energy $h\nu$ according to the following relation

$$\alpha(\nu) = \alpha_o exp(h\nu/E_e), \tag{5}$$

where α_o is a constant and E_e is interpreted as the width of the tails of localized states in the forbidden gap. In general, E_e represents the degree of disorder and defects in amorphous semiconductors [32]. Therefore, plotting the dependence of $\ln\alpha$ versus $h\nu$ gives straight line as shown in Fig.8. The inverse of the slope gives the band tail width, E_e, of the localized state. The effect of annealing temperature on E_e for the studied composition is shown in Fig. 7. It is observed that E_e increases with increasing the annealing temperature. The decrease in the optical energy

gap, E_g, and the increase of localized states tail, E_e, with increasing annealing temperature have been successfully analyzed on the basis of the theory proposed by Mott and Davis theory [17]. The thermal annealing above the glass transition temperature T_g is known to be important for including crystallization in semiconductor chalcogenide glasses [16, 33, 34].

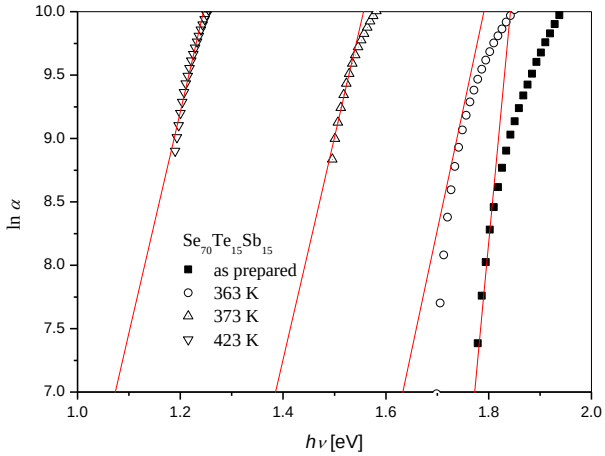

Fig. 8. Plot of ln(α) versus hv for $Se_{70}Te_{15}Sb_{15}$ thin film at different annealing temperature.

The SEM and the XRD indicated amorphous crystalline transformation after annealing at temperature higher than T_g as shown in Figs. (2, 3). During annealing at temperature higher than T_g, the indirect optical energy gap decreases and the width of localized states tails increases with the increase of the annealing temperature. These results can be interpreted by assuming the production of surface dangling bonds around the crystallites [35] during the process of the crystallization.

It has been suggested by many authors [15, 22, 36] that nearly ideal amorphous solids crystallize under heat treatment. During the process of crystallization dangling bonds produced around the surface of the crystallites. Further increasing of the annealing temperature causes the crystallites to breakdown [37] into smaller crystals thereby increasing the number of surface dangling bonds. The increasing of the dangling bonds is responsible for the formation of some types of defects in highly polycrystalline solids. As the number of dangling bonds and defects increase with increasing the annealing temperature, the concentration of localized states in the band structure increases gradually. Hence, the heat treatment of the films causes an increase in the energy width of localized states thereby reducing the optical energy gap.

3.2.2 Dispersive optical constant

The values of the refractive index, n, and extinction coefficient, k_{ex}, has been calculated using the following relation [38]

$$R = [(n-1)^2 + k_{ex}^2]/[(n+1)^2 + k_{ex}^2], \tag{6}$$

where

$$k_{ex} = \frac{\alpha\lambda}{4\pi}, \tag{7}$$

The spectral dependence of the refractive index, n, and extinction coefficient, k_{ex}, on the wavelength for as-deposited and annealed $Se_{70}Te_{15}Sb_{15}$ thin films are shown in Fig. 9(a, b). The values of n have a maximum value, n_{max}, at wave length λ_c which is shifted towards longer wavelength as the annealing temperature increased as shown in Fig. 9(a). Furthermore, the extinction coefficient, k_{ex}, decreases with increasing the wavelength. In general, the values of n and K_{ex} increased with increasing the annealing temperature. The chalcogenide glasses always contain

a high concentration of unsaturated bonds or defects. These defects are responsible for the presence of localized states in the amorphous semiconductor. During thermal annealing at temperature below the crystallization temperature, the unsaturated defects are gradually annealed out producing a large number of saturated bonds. The reduction in the number of unsaturated defects decreases the density of localized states on the band structure. Consequently, it increases the refractive index and extinction coefficient. Furthermore, the increasing in n and k_{ex} can be interpreted by an increase in the particle size with increasing the annealing temperature [39].

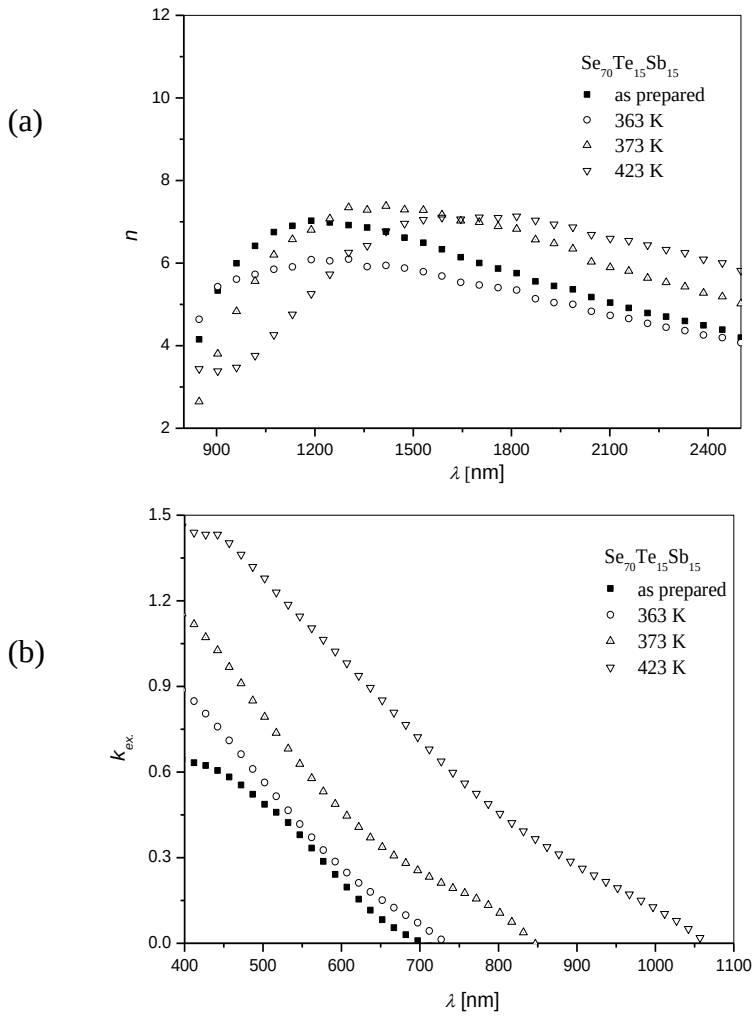

Fig. 9. The variation of a) refractive index, n, and b) extinction coefficient, k_{ex}, with wavelength for the $Se_{70}Te_{15}Sb_{15}$ thin films at different annealing temperature for 1 h.

The dispersion of refractive index, n, may be analyzed using the concept of the single-oscillator and can be expressed by Wemple-Didomenico relationship (WDD) [40, 41]

$$n^2 = 1 + \frac{E_o E_d}{E_o^2 - (h\nu)^2} \quad , \tag{8}$$

where E_o is the single-oscillator energy for electronic transitions (also called average energy gap) and E_d is the dispersion energy, which measure the strength of interband optical transitions. The dispersion parameters E_d and E_o can be obtained according to Eq. 8 by plotting $(n^2\text{-}1)^{-1}$ versus $(h\nu)^2$ as shown in Fig. 10. The values of E_d and E_o have been determined from the slopes and the intersection of the straight lines with $(n^2\text{-}1)^{-1}$ axis. The obtained values of E_d and E_o for the as-deposited and annealed $Se_{70}Te_{15}Sb_{15}$ thin films are listed in Table 2. It is clear that the value of E_o

decrease while the value of E_d increase with increasing the annealing temperatures. These results could be attributed to an increasing the rate of diffusion of atoms of the films with increasing the annealing temperature. The increase in the diffusion rate with increasing the annealing temperature gives more number of atoms at interstitial sites, thereby leading to impurity type scattering centers [23, 42, 43]. In our results it is found that $E_o \simeq E_g$ which is nearly in agreement with the relation of Ticha and Tichy [44].

Table 2 Optical parameters of $Se_{70}Te_{15}Sb_{15}$ thin films.

Ann. Temp. [K]	E_g **[eV]**	E_e **[eV]**	E_d **[eV]**	E_o **[eV]**	ε_l	ε_∞	$N/m^* \times 10^{57}$ **[m^{-3} Kg^{-1}]**
As	1.55	0.023	26.04	1.19	40.51	22.88	4.41
363	1.53	0.053	19.55	1.15	33.88	17.97	3.39
373	1.27	0.0571	27.52	1.06	55.16	26.97	5.88
423	1.01	0.0572	28.93	1.02	67.13	29.38	6.46

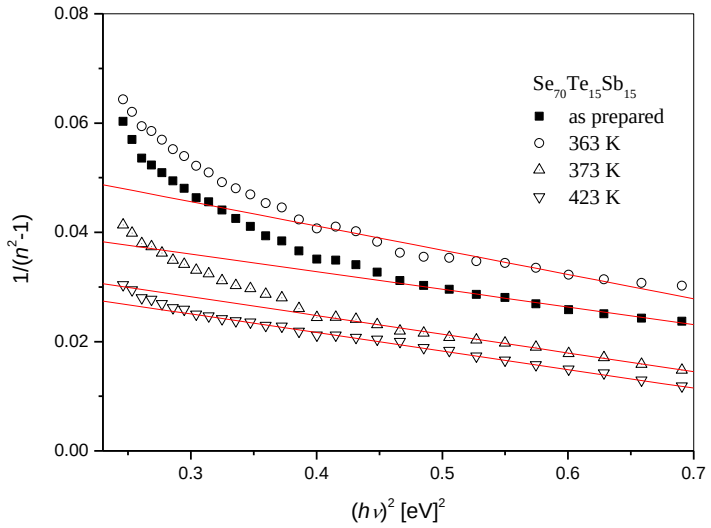

Fig. 10. $(n^2 - 1)^{-1}$ as a function of $(h\nu)^2$ for annealed $Se_{70}Te_{15}Sb_{15}$ thin films at different temperature for 1 h.

3.2.3 Determination of the high frequency dielectric constants:

For a better understanding of the optical properties of the as- deposited and annealed films, the data of refractive index dependence on photons energy or wavelength we analyzed via two procedures. The first one includes the contribution of free carriers and the lattice vibration models of dispersion. In this method the relation between the lattice high frequency constant, ε_l, and the refractive index, n, is given by the following relation [45]

$$n^2 = \varepsilon_l - \left(\frac{e^2}{4\pi^2 \varepsilon_o C^2}\right)\left(\frac{N}{m^*}\right)\lambda^2, \tag{9}$$

where e the electronic charge, N/m^* is the ratio of the free carrier concentration to the effective electron mass m^*, ε_o is the free space dielectric constant and c is the speed of light. Fig. 11 show the plot of n^2 versus λ^2 for $Se_{70}Te_{15}Sb_{15}$ thin films. Extrapolating the linear part of this dependence to zero wavelength gives the value of ε_l and from the slopes of these lines the values of N/m^* was obtained. It is clear from Table 2, the values of ε_l and N/m^* increases with increasing the annealing temperatures. The increasing of ε_l with increasing the annealing temperatures can be

attributed to the increase of the free carrier concentration. In general, it can be concluded that the high frequency dielectric constant ε_l and the ratio N/m^* are related to the internal structure.

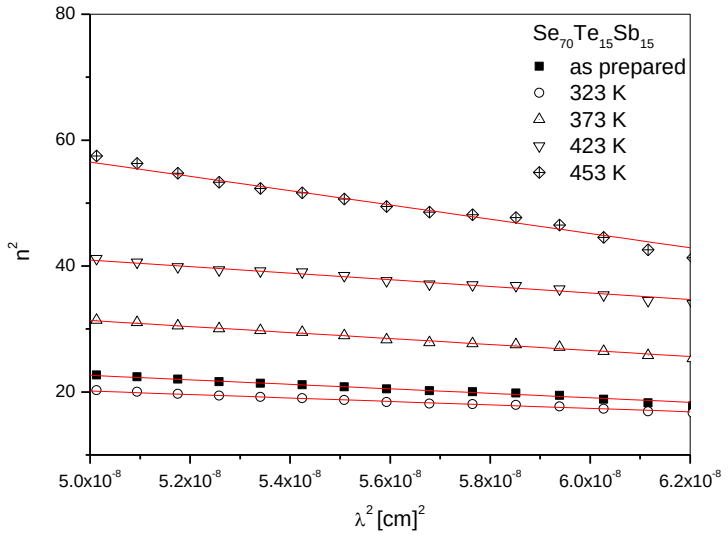

Fig. 11. n^2 as a function of λ^2 for as-deposited and annealed $Se_{70}Te_{15}Sb_{15}$ thin films at different temperature for 1 h.

The second procedure for calculating ε_∞ is based on the dispersion arising from the bound carriers in an empty lattice. In this procedure, $\varepsilon_\infty (= n_\infty^2)$ can be deduced by applying the following classical dispersion relation using the single term sellmeir oscillation [46]

$$\frac{n_\infty^2 - 1}{n^2 - 1} = 1 - \left(\frac{\lambda_0}{\lambda}\right)^2, \tag{10}$$

where n_∞ is the long wavelength refractive index and λ_o is the average oscillator wavelength . Plots of $(n^2\text{-}1)^{-1}$ versus λ^{-2} for $Se_{70}Te_{15}Sb_{15}$ thin films are shown in Fig. 12. The deduced values of ε_∞ according to Eq. 10 are listed in Table 2. It is clear that the values of ε_l are greater than ε_∞ . This behavior can be attributed to the increasing in the free carrier concentration [47].

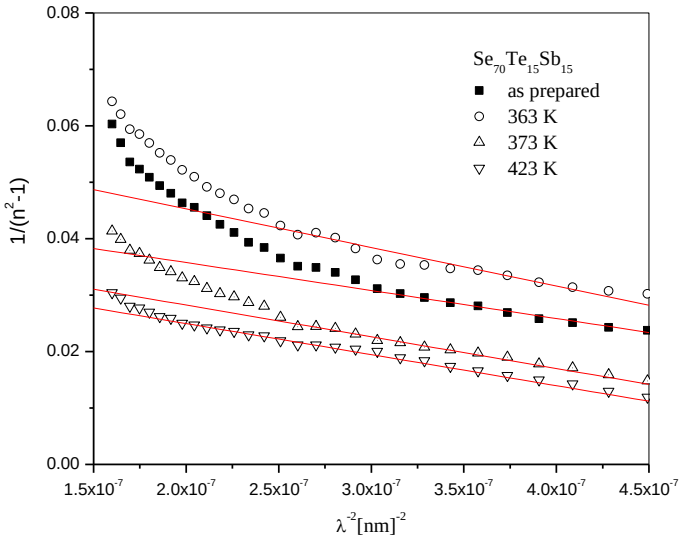

Fig. 12. $(n^2 - 1)^{-1}$ as a function of λ^{-2} for as-deposited and annealed $Se_{70}Te_{15}Sb_{15}$ thin films at different temperature for 1 h.

4. Conclusions

From the above results and discussion, one can conclude that the optical absorption measurements for as-deposited and annealed films for $Se_{70}Te_{15}Sb_{15}$ indicated that the absorption mechanism is due to indirect transition.

Thermal annealing between the glass transition and crystallization caused a decrease in the optical energy gap and increase the width of localized states. This behavior is attributed to producing more surface dangling bonds around the formed crystallites during the crystallization process.

The refractive index, n, and extinction coefficient, k_{ex}, increased with increasing the annealing temperature.The results indicate that the optical parameters E_o, E_d, ε_l, ε_∞ and N/m^* are sensitive to heat treatment.

The transformation from amorphous to crystallization was studied using XRD and SEM. The results show that the average crystallite size increased whereas the dislocation density and strain decreased with increasing the annealing temperature.

As a result of this property, the films good materials for the construction of poultry roofs and walls for the protection of young chicks from the sun's burning due to UV radiation while the admittance of infrared radiation helps to warm the inside of the poultry house which is needed for young chicks. The films are also suitable for eye glass coating for the protection of the skin around the eye from UV radiation.

References

[1] A. Elshafie and A, Abdel-All, Phys. B **269**, 69 (1999).
[2] K. Abe, H. Takebe and K. Maronaga, J. Non-Cryst. Solids, **212**, 143 (1997).
[3] D.P Machewirth, K Wei, V Krasteva, R Datta, E Snitzer and G.H Sigel Jr., J. Non-cryst. Solids **213-214**, 295 (1997).
[4] K. Wei, D. P. Machewirth, J. Wenzel, E. Snitzer and G. H. Sigel Jr., J. Non-Cryst. Solids, **182**, 257 (1995).
[5] J. Rowlands and S. Kasap, Phys. Today 50 (1997) 24.
[6] J. M. Harbold, F. O. Ilday, F. W. Wise and B. G. Aitken, IEEE Photon. Tech. Lett. **14**, 822 (2002).
[7] A. Onozuka and O. Oda, J. Non-Cryst. Solids **103**, 289 (1988).
[8] M. A. Abdel-Rahim, A. Gaber, A. A. Abu- Sehly and N. M. Abdelazim, J. Non-cryst. Solids **376**, 158 (2013).
[9] M. A. Abdel-Rahim, J. Non-cryst. Solids **241**, 121 (1998).
[10] Ravi Chander, R, Thangaraj, Thin Solid Films **520**, 1757 (2012).
[11] K. A. Aly, H. H. Amer and A. Dahshan, Materials Chemistry and Physics **113,** 690 (2009).
[12] M. A. Abdel-Rahim, Physica B **239**, 238 (1997).
[13] Sunil kumar and Kedar Singh, Physica B **406**, 1519 (2011).
[14] M. A. Abdel-Rahim, M. M. Hafiz M. M. El-Nahass and A. M. Shamekh Physica B **387,** 383 (2007) .
[15] M. A. Abdel-Rahim, J. Phys. Chem. Solids **60**, 29 (1999).
[16] F. S. Al-Hazmi, Physica B **404**, 1354 (2009).
[17] N. F. Mott and E. A. Davis, Electronic Processes in Non-crystalline Materials, Clarendon Press, Oxford, (1979) 428.
[18] P. Scherrer, Mathematisch-Physikalische Klasse **2**, 98 (1918).
[19] S. B. Qadri, E. F. Skelton, D. Hsu, A. D. Dinsmore, J. Yang, H. F. Gray, B. R. Ratna, Phys. Rev. B **60**, 9191 (1999).
[20] S. Venkatachalam, D. Mangalaraj and Sa. K. Narayanadass, Physica B **393**, 47 (2007).
[21] H. MahfozKotb, M. A. Dabban, F. M. Abdel-Rahim, A. Y. Abdel-latif and M. M. Hafiz, Physica B **406**, 1326 (2011).
[22] M. A. Abdel-Rahim, A. Y. Abdel-latif, M. Rashad and N. M. Abdelazim, Materials Science in Semiconductor Processing **27**, 27 (2014).

[23] M. A. Abdel-Rahim, M. M. Hafiz and A. Elwhab. B. Alwany, Opt. Laser Technol. **44,** 1116 (2012).
[24] B. Alterkop, B. Alterkop, N. Parkansky, S. Goldsmith, and R.L. Boxman, J. Phys. D: Appl. Phys. **36**, 553 (2003).
[25] M. I. Abd-Elrahman and M. M. Hafiz, J. Alloys & Compd **551**, 562 (2013).
[26] J. I. Pankove, Optical process in semiconductors, (Dover Publications, Inc. New York 1971) p.103.
[27] E. A. Davis and N. F. Mott, Philos. Mag. **22**, 903 (1970).
[28] V. K. Saraswat and V. Kishore, Chalcogenide Lett. **4**, 61 (2007).
[29] K. B. Kale andC. D. Lokhande, Appl. Surf. Sci. **252**, 929 (2005).
[30] S. Venkatachalam, D. Mangaloraj and Sa. K. Narayandass, Physica B **47**, 393 (2007).
[31] F. Urbach, Phys. Rev. **92**, 1324 (1953).
[32] J. A. Olley, Solid State Commum. **13**, 1437 (1973).
[33] M. A. Abdel-Rahim, A. Y. Abdel-latief, A. El-Korashy and M. A. Sabet, Mater. Trans. **51**(3) 428 (2010).
[34] A. A. El-Sebaii, Shamshad A. Khan, F. M. Al-Marzouki, A. S. Faidah, A. A. Al-Ghamdi, J. Luminescence **132**(8), 2082 (2012).
[35] S. Chaudhari, S. K. Biswas, A. Chaudhary and K. Goswami, J. Non-Cryst.Solids, **54**, 179 (1983).
[36] S. Shigetomi, H. Ohkubo and Ikari, Thin Solid Films **199**, 215 (1991).
[37] S. Hasegawa and M. Kitagawa, Solid State Commum. **27**, 855 (1978).
[38] F. Yakuphanoglu, M. Kandaz, M.N. Yaraşır and F. B. Şenkal, physica B **393**, 235 (2007).
[39] E. Bertran, A. Lousa, M. Varela, M. V. Garcia, J. L. Morenza, Solar Energy Mater. **17**, 55 (1988).
[40] S. H. Wemple and M. Didomenico, Phys. Rev. B **3**, 1338 (1971).
[41] S. H. Wemple, Phys. Rev. B **7**, 3767 (1973).
[42] M. M. Malik, M. Zulfequar, A. Kumar and M. Husain, J. Physics; Condensed Matter **4**, 8331 (1992).
[43] V. Damodara Das and Ramesh Chandra Mallik, Material Research Bulletin **37**, 1961 (2002).
[44] H. Tichá and L. Tichý, Journal of Optoelectronics and Advanced Materials **4**(2), 381 (2002).
[45] J. N. Zemel, J. D. Jensen, and R. B. Schoolar, Phys. Rev. **140**, A330 (1965).
[46] A. K. Wolaton, T. S. Moss, Proc. Roy. Soc. **81**, 5091 (1963).
[47] F. Yakuphanoglu, C. Viswanathan, J. Non-Cryst. Solids **353**, 2934 (2007).